Kinetics and Mechanisms of Acrylamide Polymerization from Absolute, Online Monitoring of Polymerization Reaction

Ahmet Giz,[‡] Huceste Çatalgil-Giz,[†,§] Alina Alb,[†] Jean-Luc Brousseau,[†] and Wayne F. Reed*[,†]

Physics Department, Tulane University, New Orleans, Louisiana 70118; and Istanbul Technical University, Fen Edebiyat Fakültesi, 80626 Maslak, Istanbul, Türkiye

Received May 11, 2000

ABSTRACT: An automatic, continuous, online monitoring technique was used to follow the polymerization of acrylamide under a variety of temperature and initiator conditions, without chromatographic columns. The technique furnishes, as a function of time, the weight-average polyacrylamide mass M_w, the monomer conversion, reduced viscosity, and certain measures of polydispersity. After a complex initial phase following initiator addition, wherein impurities competed with monomer for free radicals, monomer conversion followed a first-order decay during most of the subsequent reaction. For fixed monomer concentration, at every point in conversion beyond very early points, M_w was proportional to the inverse square root of the initiator concentration. Furthermore, the monomer decay time also scales in the same way, and M_w vs conversion is linear during most of the conversion, with a negative slope. Hence, the overall reaction scheme falls within the quasi-steady state approximation (QSSA) of ideal polymerization kinetics. The rate constant for initiator decay, as well as the ratio of propagation rate constant squared to termination rate constant were determined. The activation energy for the potassium persulfate initiator decomposition was also determined. Deviations from the ideal kinetics at early and late conversion are rationalized by existing models. Using a technique for determining instantaneous polydispersity from the derivative of M_w, it was possible to follow the evolution of the polydispersity for the polyacrylamide reactions.

Introduction

Florenzano et al.[1] recently introduced a technique for continuous, absolute, online monitoring of polymerization reactions. The method furnishes the time dependent signature of cumulative weight-average mass M_w, and *z*-average radius of gyration $\langle S^2 \rangle_z$, as well as the polymer reduced viscosity η_r, and monomer conversion *f*. More recently, several approaches have been taken to determine the evolution of the polydispersity during online monitoring.[2]

In this work, the online monitoring technique is applied to the case of polyacrylamide (PAAm). The aim is to analyze the kinetics of the data generated by online monitoring and to assess online measures of polydispersity. This type of monitoring should provide new opportunities for critical assessment of models for polymerization kinetics, as well as useful tools for practical control of polymerization reactions.

We attempt to find the simplest kinetic scheme consistent with the data and, from this, determine the portion of the initiator decay constant leading to chain propagation and the relationship between the propagation and termination rate constants. The temperature dependence of trends and rate constants is also explored, as well as the evolution of polydispersity during the reactions. The simplest explanations for deviations from the basic model are examined in light of reactions competing for free radicals at early and late points in the monomer conversion process.

* Correspondence author.
† Tulane University.
‡ Istanbul Technical University.
§ On leave from Istanbul Technical University, Fen Edebiyat Fakültesi.

A detailed treatise on polymerization kinetics with extensive bibliography is given by Dotson et al.[3] Other valuable texts include those by Rodriguez,[4] Odian,[5] and Bamford.[6] Several formalisms exist for predicting conversion rates and the evolution of instantaneous and cumulative mass distributions. These include discrete transformations,[7,8] sequential solutions and direct integration of rate equations, analytical solutions for distribution moments,[9] and statistical approaches.

The quasi-steady state approximation (QSSA) is often assumed to hold in many chain-growth polymerizations, and it yields tractable solutions to the rate equations. It is by no means universal, however, and even the straightforward PVP reaction, initiated by hydrogen peroxide, recently studied by the real-time technique showed fundamental deviations from the QSSA.[1] Diffusion-controlled phenomena, e.g., the Trommsdorf effect,[10] can change rates as reactions proceed and further complicate kinetic models.

Previous Work on Monitoring Polymerization Kinetics. Monitoring kinetics of polymerization reactions requires that measurements be made either periodically or continuously on a reacting solution. One of the first works was due to Flory,[11] who manually withdrew aliquots from a glycol/dibasic acid polyesterification reaction every 10 min and performed a KOH titration to estimate molecular weights and rate constants. Bresler et al.[12] made periodic ESR measurements to follow radical concentrations in homogeneous polymerization reactions of methyl methacrylate and vinyl acetate. Shen and Tian subsequently improved on the ESR technique and simultaneously measured radical concentration and monomer conversion in methyl methacrylate polymerization at intervals a few minutes apart.[13] Ballard and van Lienden[14] used literature values of polymer densities to estimate initial poly-

10.1021/ma000815s CCC: $20.00
Published on Web 02/02/2001

merization rates of vinyl monomers by metal compounds using a dilatometer.

Real-time monitoring of polymerization is a more recent development. Infrared,[15,16,17,18,19,20,21] UV,[22,23] and fluorescence monitoring[24] are proving useful for measurements of monomer conversion. Fluorescence techniques are used for monitoring epoxy curing reactions.[25] IR studies have been used to estimate rheological properties,[26] whereas direct rheological techniques are used to estimate molecular weight online.[27,28,29] Monitoring post-pulse processes in laser-induced polymerization has been recently reported.[30] Monitoring of laser-induced surfactant vesicle polymerization, in which laser flash photolysis was used to follow monomer conversion rates, has been detailed.[31,32]

Besides techniques used for monitoring monomer conversion and polymer properties, several online methods for measuring colloid particle evolution have been reported. These include frequency domain photon migration[33] and dynamic light scattering for particle size distributions.[34] Online ultrasonic techniques are becoming useful for monitoring changes in emulsion properties.[35,36] A recent work provides a means of simultaneously measuring the evolution of coexisting polymers and colloid populations using heterogeneous time-dependent static light scattering.[37]

Finally, significant effort is being made in addressing the stability and calibration problems involved in using sensitive detectors,[38] and global concerns of overall detector integration have been addressed, including the use of neural networks.[39,40]

Acrylamide Polymerization. A review of polyacrylamide preparation and properties was made by Kulicke et al.[41] The initiation step is considered to involve two reactions. The first is the production of the free radicals with rate constant k_d

$$I_2 \xrightarrow{k_d} 2I^* \tag{1}$$

where I_2 is the initiator and I* the primary radical formed by initiator decomposition.

The second initiation step is the production of the first monomer radical R_1 by combination of I* with monomer m, with rate constant k_i

$$I^* + m \xrightarrow{k_i} R_1 \tag{2}$$

In the case of persulfate initiated polymerization of acrylamide there are two species that can start polymerization, sulfate radical- ion and the hydroxyl radical:

$$S_2O_8^{2-} \rightarrow 2\ SO_4^{-}*$$

$$SO_4^{-}* + H_2O \rightarrow HSO_4^{-} + *OH$$

Radicals form in these two reactions and initiate free radical polymerization. End group studies have shown both sulfate and hydroxide groups at the ends of acrylamide chains.[6] Since the hydroxyl radical is also an efficient initiator, the transfer of activity from the persulfate radical to it does not have a large impact on the kinetics.

In the case of persulfate/thiosulfate redox couple reactions, thiosulfate is relatively unreactive in initiating the polymerization, but increases the rate by rapid production of sulfate radical ions through the following reaction.[6]

$$S_2O_8^{-2} + S_2O_3^{-2} \rightarrow SO_4*^{-} + SO_4^{-2} + S_2O_3*^{-}$$

Propagation ensues with rate constant k_p (assumed equal for all chain lengths).

$$R_1 + m \xrightarrow{k_p} R_2 \tag{3}$$

Termination occurs mainly by disproportionation.[42]

$$R_m + R_n \xrightarrow{k_t} P_m + P_n \tag{4}$$

Kinetics of Polymerization and the Quasi-Steady-State Approximation (QSSA). The initiator concentration $[I_2]$ disappears according to the first-order expression

$$[I_2] = [I_2]_0 \exp(-k_d t) \tag{5}$$

The rate equations for monomer concentration [m], and propagating radical [R], are

$$d[R]/dt = 2Fk_d[I_2] - k_t[R]^2 \tag{6a}$$

where F is the fraction of radicals that lead to chain propagation. Here it is assumed that eq 1 is rate limiting for producing propagating radical, not eq 2. Otherwise

$$d[R]/dt = k_i[I^*][m] - k_t[R]^2 \tag{6b}$$

Here the termination constant adheres to the definition used by Dotson et al.[3] and Bamford[6] and is twice the value used by Odian.[5] The rate equation for monomer concentration is (when eq 6a holds)

$$d[m]/dt = -2Fk_d[I_2] - k_p[R][m] \sim -k_p[R][m] \tag{7}$$

The quasi-steady-state approximation is

$$d[I^*]/dt = d[R]/dt \sim 0 \tag{8a}$$

Under this approximation, radical concentrations are given by

$$0 = d[R]/dt = 2Fk_d[I_2] - k_t[R]^2 \tag{8b}$$

so that

$$[R] = \sqrt{\frac{2Fk_d[I_2]}{k_t}} \tag{9}$$

If $[I_2]$ decreases negligibly during converion, then monomer disappears in a first-order process

$$[m] = [m]_0 e^{-\kappa t} \tag{10}$$

where the rate constant κ is given by

$$\kappa = k_p[R] \tag{11}$$

Materials and Methods

Online Monitoring of Polymerization Reactions. The continuous, absolute, online monitoring technique was described in detail in ref 1. Supporting Information to this article contains additional details. Briefly, it uses automatic, continuous withdrawal of a small stream of reactor solution, which is

continuously mixed with a pure solvent from a reservoir, to produce a very dilute polymer solution, on which useful light scattering and viscometric measurements can be made.

An ISCO 2360 programmable mixer was used to continuously withdraw nominal, preset percentages from the reactor and solvent reservoir, set at 4% and 96%, respectively. The flow rate was 2 mL/min, so that about 5 mL of reactor solution was consumed during the course of a typical reaction.

The diluted solution was continuously pumped through a detector train consisting of (1) a home-built, seven angle absolute scattering intensity monitor (or time dependent static light scattering, TDSLS), details of which have been recently published,[43] (2) a home-built, single capillary viscometer, which has also been described in detail,[44] (3) a Shimadzu SPD-10AV ultraviolet (UV) absorption spectrophotometer, and (4) a Waters 410 refractive index (RI) detector. The UV detector, with a 0.1 mm path length cell monitoring UV absorption at 225 nm, followed the disappearance of monomer, whereas the RI detector provided total polymer and monomer concentration in the detector stream. Together, these two detectors yield the instantaneous concentration of polymer and monomer in the detector stream as long as the refractive index increment dn/dc is known for both monomer and polymer. For AAm and PAAm, the values of dn/dc were found to be 0.1509 and 0.1939, respectively.[45]

In conjunction with the polymer concentration c, determined this way, the TDSLS monitor allows computation of absolute M_w and $\langle S^2\rangle_z$, using the well-known Zimm approximation,[46] valid for $q^2\langle S^2\rangle_z \ll 1$

$$\frac{Kc}{I(q,c)} = \frac{1}{M_w}\left(1 + \frac{q^2\langle S^2\rangle_z}{3}\right) + 2A_2c \tag{12}$$

where $I(q,c)$ is the excess Rayleigh scattering ratio (total scattering of polymer solution, minus solvent scattering), and K is an optical constant, given for vertically polarized incident light by

$$K = \frac{4\pi^2 n^2 (\mathrm{d}n/\mathrm{d}c)^2}{N_A\lambda^4} \tag{13}$$

where n is the solvent index of refraction, λ is the vacuum wavelength of the incident light, q is the scattering wave vector $q = (4\pi n/\lambda)\sin(\theta/2)$, and θ is the scattering angle. It was found that PAAm with $M_w = 10^6$ g/mol yields $\langle S^2\rangle_z \sim 500$ Å, a value which is reasonable for the use of eq 12 over the angular range of the scattering detector.

A_2 was determined independently in separate Zimm plot measurements of final products of different M_w. It was found to be 5.69×10^{-4} cm^3-mol/g^2 ± 2.8%. Hence, determination of $I(q,c)$ and c at every point in time allows M_w and $\langle S^2\rangle_z$ to be computed from the above equation. Reference 1 describes error bars in M_w due to the uncertainty in A_2, represented by ΔA_2, which amount to

$$\frac{\Delta M_w}{M_w} = 2cM_w\Delta A_2 \tag{14}$$

For data in this work, the error in M_w due to the A_2 correction is at most 1.8%. Hence, this source of systematic error is small.

The viscometer was a single capillary mounted via T-connectors to a Validyne Engineering differential pressure transducer. The voltage output of the transducer is proportional to the pressure drop across the capillary, which in turn is proportional to total solution viscosity. Total solution viscosity is

$$\eta = \eta_s\lfloor 1 + [\eta]c + k[\eta]^2c^2\rfloor \tag{15}$$

where η_s is the pure solvent viscosity, $[\eta]$ is the intrinsic viscosity of the polymer, and k is a constant related to the hydrodynamic interactions between polymer chains, usually around 0.4 for neutral, coil polymers.[47] The intrinsic viscosity is the extrapolation to zero concentration and zero shear rate of the reduced viscosity η_r. η_r can be computed directly from the voltage of a single capillary viscometer at every point in time t, without need of an instrumental calibration factor, in terms of the viscometer baseline voltage V_b (when pure solvent flows) and the concentration at point t, $c(t)$:

$$\eta_r(t) = \frac{V(t) - V_b}{c(t)V_b} \tag{16}$$

The average shear rate is about 860s^{-1} for $Q = 1$ mL/min and $R = 0.0254$ cm. Fortunately, shear effects diminish with diminishing c.

The temperature inside the reactor was monitored with a k-type thermocouple.

Polymerization Reactions. Acrylamide (99+ %, electrophoresis grade), potassium persulfate (hereafter persulfate), and sodium thiosulfate (thiosulfate) were from Aldrich, and were used as received. Water was deionized and filtered by a 0.22 μm filter in a Modulab UF/UV system. In the polymerization reactions, 20 mL of acrylamide (AAm) solution were placed in a round-bottomed flask and purged for 30 min by N_2 bubbling. The thermocouple and Teflon sampling tube were inserted in the reaction flask, which was put in a temperature-stabilized water bath. The solution was magnetically stirred throughout.

The mixing pump was used to continuously withdraw nominally 4% of the liquid from the reaction vessel and mix this with 96% pure water from reservoir. The diluted solution flowed continuously through the detectors, which were stabilized before the initiator was added. After stabilization, 5 mL of persulfate solution in degassed water was added to the reaction flask. The reaction conditions for different experiments are given in Table 1. After the reaction was over the polymer in the reactor was precipitated by methanol, dried, and measured by a size exclusion chromatography (SEC) system with coupled RI, UV−viscometer, and static light scattering detection, previously described.[48]

Results and Discussion

Table 1 is a summary of all potassium persulfate initiated acrylamide polymerizations performed, including those using sodium thiosulfate/potassium persulfate initiated experiments. Special emphasis was given to the potassium persulfate initiated system, and it was studied for different initiator concentrations at different temperatures. Also shown in Table 1 are the linear fit parameters to M_w vs conversion f, discussed below, and final online values of M_w and η_r, and, when available, the corresponding values obtained by SEC.

Figure 1 shows typical raw data signals for a PAAm reaction (B2, Table 2), including the viscometer, UV, RI, and TDSLS signal at $\theta = 90°$. Significant features include the stable detector plateau when pure solvent is being pumped, the rise of the RI and UV detectors when pure monomer is pumped prior to addition of initiator, and the point at which initiator is injected at 1283 s. The segments corresponding to pure H_2O, 4% AAm monomer, and the postreaction flush with H_2O are indicated, as well as the point where initiator was added. The lag time between adding initiator and observing the reaction on the detectors is 458 s. As the reaction proceeds, the UV signal decreases, showing the conversion of monomer to polymer, and the TDSLS and viscometer signals increase as polymer is produced. A downward dip in the RI indicates that the reactor liquid is becoming more viscous and the mixing pump cannot pull the preset percentage. This does not hamper the data analysis, since the polymer concentration is being

Table 1. Conditions for the Acrylamide Polymerization[a]

reaction no.	$M_{w,final}$ on-line measured	$M_{w,final}$ SEC	persulf/Am (g/g)	T (°C)	by SEC M_w/M_n	by SEC M_z/M_w	η_{red} SEC	η_{red} online	intercept; slope of M_w vs f	−int./slope
A1	130000 ± 4%	170000 ± 4%	0.380	70	3.8	3.0	132	102	2.291e5; −1.128e5	2.03
A2	163000 ± 4%		0.189	70				106	3.338e5; −1.770e5	1.89
A3	264000 ± 3%		0.094	70				134	5.142e5; −2.971e5	1.73
A4	420000 ± 4%		0.047	70				188	8.012e5; −4.096e5	1.96
A5	420000 ± 4%		0.047	70				176	7.812e5; −3.786e5	2.06
A6	584000 ± 4%	502000 ± 9%	0.023	70	6.9	2.4	251	240	1.058e6; −5.720e5	1.85
B1	224000 ± 3%		0.379	60				123	3.845e5; −1.747e5	2.20
B2	450000 ± 3%	462000 ± 3%	0.094	60	3.5	2.5	240	224	8.261e5; −4.109e5	2.01
B3[b]	120000 ± 3%	130 000 ± 4%	0.094	60	11.6	3.1		70	2.561e5; −1.517e5	1.69
B4	240000 ± 3%		0.094	60				125	5.409e5; −3.583e5	1.51
B5	720000 ± 4%	709000 ± 3%	0.025	60	2.5	2.3	298	293	1.544e6; −9.076e5	1.70
B6[d]	900000 ± 5%	890000 ± 4%	0.026	61	3.1	2.1	256	264	2.0521e6; −1.241e6	1.65
C1	406000 ± 3%		0.379	50				182	7.284e5; −3.362e5	2.17
C2	900000 ± 5%		0.094	50				265	1.38e6; −3.21e5	4.30
C3[c]	123000 ± 3%		0.094	50				78	2.712e5; −1.584e5	1.71

[a] Am concentration in reactor was 0.034 g/mL, except for B4, which was 0.020 g/mL [b] Thiosulfate/Am (g/g) was 0.049. [c] Thiosulfate/Am (g/g) was 0.054. [d] Aliquots withdrawn during reaction.

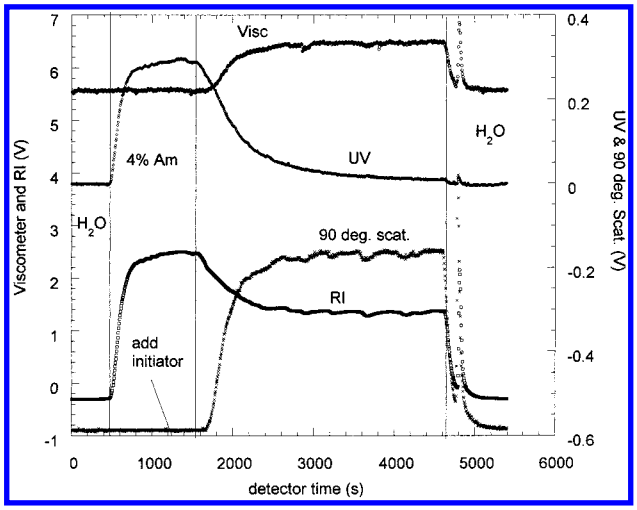

Figure 1. Typical raw data signals for a PAAm reaction, including the viscometer, UV, RI, and TDSLS (at 90°) signals. This is reaction B2 in Table 1.

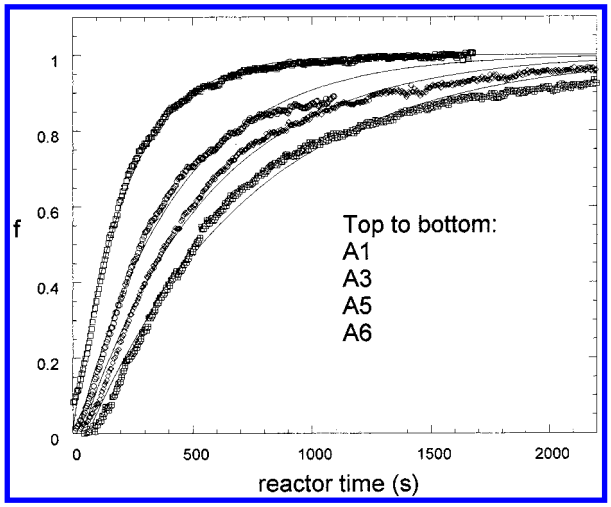

Figure 2. Monomer conversion f, vs t, for several reactions at T = 70 °C, including the first-order fit according to eq 17. Reaction designations are from Table 1.

Table 2. Kinetic Parameters for Acrylamide Polymerization

	T = 70 °C	T = 60 °C	T = 50 °C
$2Fk_d$ (s^{-1})	1.75×10^{-5}	7.56×10^{-6}	1.96×10^{-6}
k_p^2/k_t (L/[M × s])	16.7 ± 0.95	14.7 ± 1.05	10.6 ± 1.5

continuously monitored and M_w and other quantities can be computed. In this experiment, the drop in pump efficiency dominated the RI behavior, which otherwise would have increased as polymer was produced, if pump efficiency remained high, since dn/dc of the polymer is greater than that of the monomer.

Figure 2 shows monomer conversion f ($f = 1 - [m]/[m]_0$), vs reactor time for different reactions. The curves in Figure 2 can be treated approximately as first order over a significant portion of the reaction. Fits of the form

$$f(t) = 1 - e^{-\kappa(t-t_i)} \qquad (17)$$

are also shown in Figure 2, where κ is the first-order decay rate constant defined by eq 11 and t_i is an "induction period", which is related to the duration of the complex initial period before QSSA conditions are established. The fit is best for the fastest reactions, i.e., those with highest initiator concentration. The "induction period" is seen to increase for slower reactions. The ln[m] vs t curves did not show a steepening with increasing conversion. This indicates that auto acceleration[12] was absent or insignificant. This is expected as we are working in dilute solutions.

Figure 3 shows M_w vs time for reactions at T = 70 °C. The general trend is that at early times large polymer chains are produced, and these fall steadily as conversion proceeds. An exception occurs at the highest initiator concentration, where small chains are first produced, M_w then increases, reaches a maximum, and then decreases like in the other reactions. Figure 4 shows M_w vs f for the reactions at T = 60 °C.

Because the online monitoring technique has only recently been introduced, it is necessary to continue to substantiate its validity with respect to traditional equilibrium characterization techniques. Hence, Figure 4 shows the values of M_w from size exclusion chromatography (SEC) for aliquots that were periodically, manually withdrawn during reaction B6, superposed on the online data. The match between M_w from the two independent techniques is very close. There are no SEC data at very early conversion, however, so that the initial steep portion of the M_w decrease is not substantiated by SEC at this point.

Further substantiation of the trends in Figures 3 and 4 is seen in Figure 5, where the online values of reduced viscosity are shown vs f for experiments at T = 70 °C.

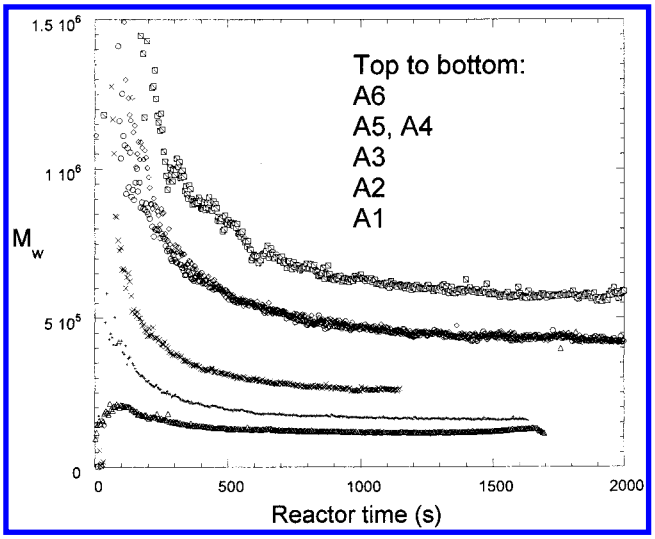

Figure 3. M_w vs reactor time for several reactions at $T = 70$ °C.

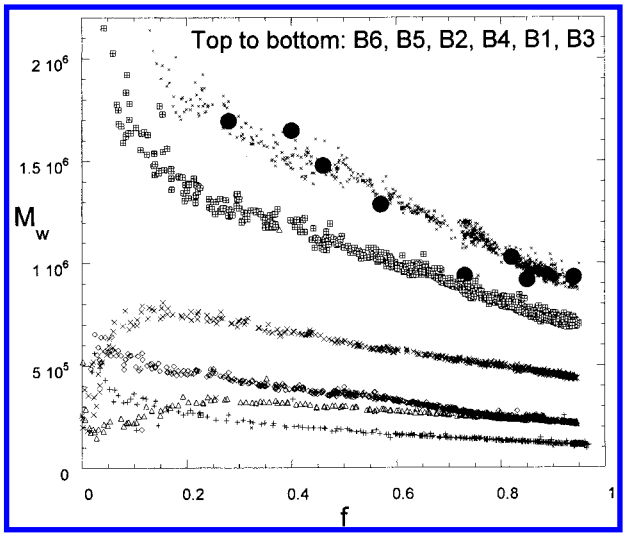

Figure 4. M_w vs f for several reactions at $T = 60$ °C. The solid circles for the top reaction (B6) correspond to the values of M_w determined by SEC for aliquots removed during the reaction.

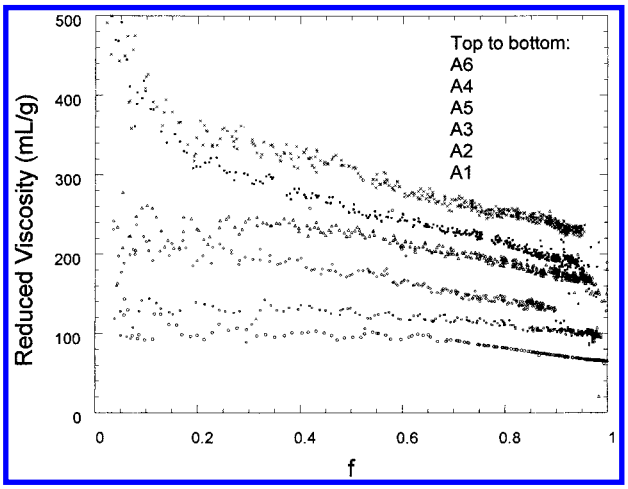

Figure 5. Reduced viscosity vs f for several reactions at $T = 70$ °C.

The two independent detectors show the same qualitative behavior for η_r and M_w.

Figure 6 shows selected raw chromatograms of the RI detector from SEC analysis of reaction B6, from which aliquots were withdrawn during the reaction and immediately cooled to room temperature and diluted to about 0.0015 g/cm^3. Shown are both the RI, from which the buildup of an increasingly polydisperse population is seen, via the increasing surface area traced out by the peak at low elution volume, and the UV signal at 225 nm, for which the monomeric content decreases as the reaction proceeds. The RI signal shows that as polymerization proceeds, the polymer distribution shifts to higher elution volumes, indicating that smaller chains are produced as the reaction proceeds, since smaller mass polymers of the same type take longer to elute than large masses. The consequent broadening of the polymer distribution is also seen. This is further corroboration of the general trend of Figures 4 and 5.

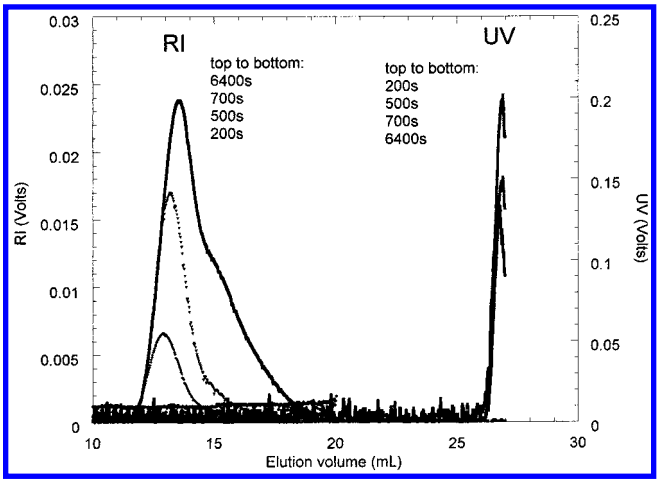

Figure 6. Raw chromatograms for SEC analysis of reaction B6, from which aliquots were withdrawn during the reaction. Both RI and UV signals are shown. The RI shows the shift to lower mass and broadening of the polymer distribution as the reactions proceeds, and the UV signal shows the disappearance of monomer.

Polydispersity Analysis. Figure 4 and Table 1 show good quantitative agreement between the online and the SEC results in terms of M_w and η_{red}, respectively. The online data themselves can be further exploited to obtain useful indices of polydispersity. The fact that $M_w(t)$ and η_{red} are changing (decreasing) in all the reactions studied (e.g., Figures 4 and 5) already indicates that the *population distribution must be broadening during polymerization.*

Polymer mass distribution determinations are normally made using fractionation techniques. Hence, it is of considerable interest to see how far the online technique (which involves no separation of polymer populations according to mass) can go in terms of yielding polydispersity information.

For the experiment involving aliquot removal, the initial SEC values of M_w/M_n of about 1.7 are close to the expected 2.0 for chain growth polymerizations in the long chain limit with termination by disproportionation, and the initial M_z/M_w values of about 1.45 are close to the expected 1.5.

Approximation to M_z/M_w Using $\langle S^2\rangle_z$ Data. The slope of Kc/I vs q^2 is a direct measure of the quantity $\langle S^2\rangle_z/M_w$. Normally, there exists a power law of the form

$$\langle S^2\rangle = AM^{\alpha} \tag{18}$$

Hence, the slope of Kc/I vs q^2 measures

$$\frac{d(Kc/I)}{dq^2} = \frac{\langle S^2\rangle_z}{3M_w} = \frac{\int AM^{\alpha+1}C(M)\,dM}{3\int MC(M)\,dM}\Bigg/\frac{\int MC(M)\,dM}{\int c(M)\,dM} \tag{19}$$

or

$$\frac{d(Kc/I)}{dq^2} = \frac{A\langle M^{\alpha}\rangle_z}{3M_w} \tag{20}$$

where $C(M)\,dM$ is the concentration of polymer in the mass interval from M to $M + dM$. For the case of an ideal random coil, $\alpha = 1$, so that the above slope is directly proportional to M_z/M_w. For a coil with excluded volume α should be in the range of 1.18 to 1.20.[49] SEC analysis on several final and intermediate products from Table 2 yielded the following relationship between $\langle S^2\rangle^{1/2}$ (cm) and M (g/mol):

$$\langle S^2\rangle(\mathrm{cm}^2) = 3.877 \times 10^{-18} M^{1.134} \tag{21}$$

Hence, the slope $d(Kc/I)/dq^2$ should be proportional to a quantity slightly higher than M_z/M_w. Even without knowledge of A and α for PAAm, the continuously monitored slope $d(Kc/I)/dq^2$ will be closely proportional to M_z/M_w.

For reaction B6, Figure 7 shows the directly computed slope, $d(Kc/I)/dq^2$, vs t, together with the SEC determinations of M_z/M_w, where the former values were scaled to the SEC values at the early times. The scaled slopes track the SEC values of M_z/M_w remarkably well, showing that $d(Kc/I)/dq^2$ can be effectively used as an index of *relative* broadening during the reactions.

Table 2 includes a column showing the ratio of final to the minimum slope (which generally occurred near early conversion times) of $d(Kc/I)/dq^2$, for those experiments where SEC determinations were made on the endproducts. This ratio follows the ratio of M_z/M_w determined by SEC fairly well.

It is pointed out that using M_z/M_w as a gauge of polydispersity evolution requires no additional experimental overhead, since the angular dependent data are automatically captured each time the detectors are read.

Approach to Polydispersity Using Derivatives of M_w. A method was recently detailed[2] for using the online data $M_w(t)$ to compute approximate polymer mass distributions and polydispersity indices as they evolve during polymerization. Since monomer conversion, defined as

$$f(t) = c(t)/[c_m(t) + c(t)] \tag{22}$$

is continuously measured online, the polydispersity indices can be represented equivalently either vs time or $f(t)$. Here, again, $c_m(t)$ is the monomer concentration and $c(t)$ the polymer concentration. In the conversion domain, the accumulated, measured weight-average mass is $M_w(f)$. The online method measures the accumulated $M_w(t)$ at each moment. For most chain growth reactions this involves an accumulation of "dead chains", which form very quickly compared to the time scale for the total conversion of monomer. When this is the case, the *instantaneous* weight-average of chains added during an interval from f to $f + df$ is given by

$$M_{w,inst}(f) = M_w(f) + f\frac{dM_w(f)}{df} \tag{23}$$

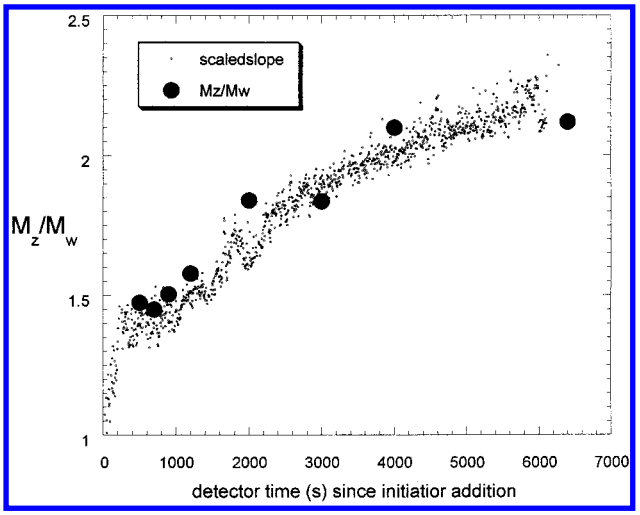

Figure 7. Slope $d(Kc/I)/dq^2$ shown to be closely proportional to a z-averaged mass $(\langle M^{\alpha}\rangle)/M_w$. The scaled value of this slope from reaction B6 tracks the SEC values of M_z/M_w remarkably well.

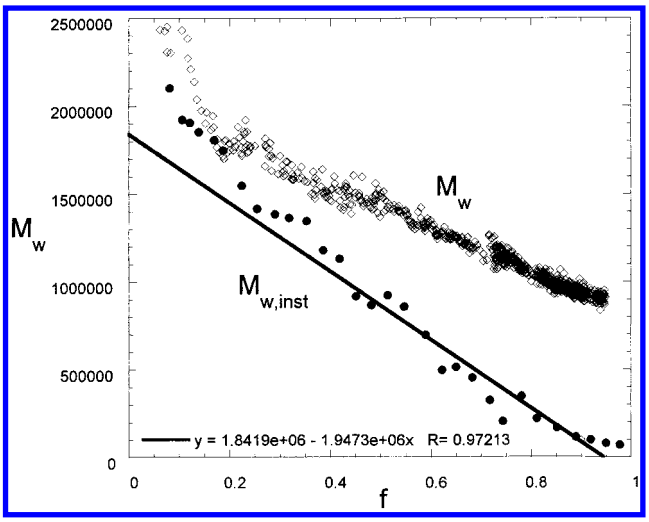

Figure 8. M_w and $M_{w,inst}$ vs conversion for reaction B6. $M_{w,inst}$ is related to the derivative of $M_w(f)$ by eq 23, as explained in the text. The slope/intercept of $M_{w,inst}$ for points for which $f >$ 0.2 is very close to the theoretical value of -1 for the QSSA.

Figure 8 shows $M_w(f)$ and $M_{w,inst}(f)$ for reaction B6, where discrete numbers of points were taken to compute $M_{w,inst}(f)$ from eq 23. The slope of $M_{w,inst}(f)$ is very close to the theoretical value of -1 in the QSSA.

$M_{w,inst}(f)$ allows immediate computation of relative $M_n(f)$ and $M_z(f)$ (or any other moment of the distribution). Hence, the relative broadening of the population during the polymerization can be immediately assessed. To obtain absolute values for $M_n(f)$ and $M_w(f)$ requires a model. For chain growth polymerizations terminating by disproportionation such as the PAAm, the instantaneous distribution is normally the geometric distribution, which, in the long chain limit yields

$$M_z{:}M_w{:}M_n = 3{:}2{:}1 \tag{24}$$

In the long chain limit, which is applicable in the case of the PAAm in all the experiments in this work, it suffices to multiply the relative $M_n(f)$ and $M_w(f)$ values by these ratios, respectively, to have a model-dependent, absolute polydispersity.

The relative polydispersities were determined using the data for $M_{w,inst}$ from Figure 8. The polydispersity

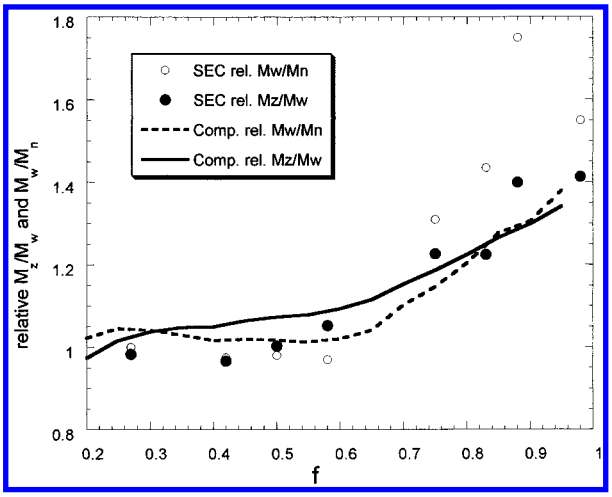

Figure 9. Relative values of SEC for M_z/M_w and M_w/M_n (reaction B6) obtained by dividing these values by their value at the first measured SEC point ($f = 0.27$). Also shown are the relative polydispersities (also with respect to their values at $f = 0.27$) computed from $M_{w,inst}$ from Figure 8.

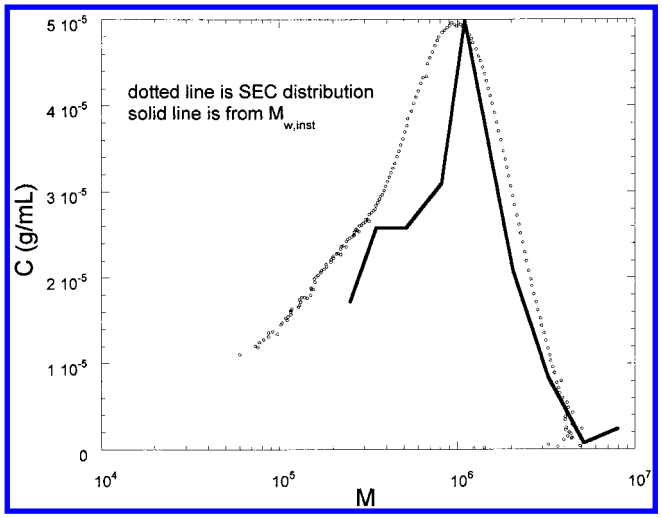

Figure 10. Final mass distribution (points) for reaction B6. Also shown (solid line) is the approximate distribution determined histogramically from the $M_{w,inst}$ in Figure 8.

data for the aliquots analyzed for B6 began at $f = 0.27$. Hence, to make a more accurate comparison of relative polydispersity, the SEC values were divided by the values at $f = 0.27$, to obtain the relative polydispersity indices for SEC. The relative values from the $M_{w,inst}$ analysis were likewise divided by their own values at $f = 0.27$, to put the comparison on an equal footing. Figure 9 shows these relative polydispersity ratios. The computed relative M_z/M_w tracks the SEC values quite well, whereas the computed relative M_w/M_n values underestimate the SEC values significantly at high conversion. These first results are encouraging for the future use of the derivative technique for following relative polydispersity.

For the purpose of visualization, $M_{w,inst}(f)$ can also be used to make histogram representations of the polymer population. Figure 10 shows the final population distribution for experiment B6, obtained from the $M_{w,inst}$-(f) curve of Figure 8, uncorrected for the polydispersity of the instantaneous population forming $M_{w,inst}$. On the same graph is shown the population distribution obtained by SEC. The derivative method is seen to capture some of the features of the more accurate distribution

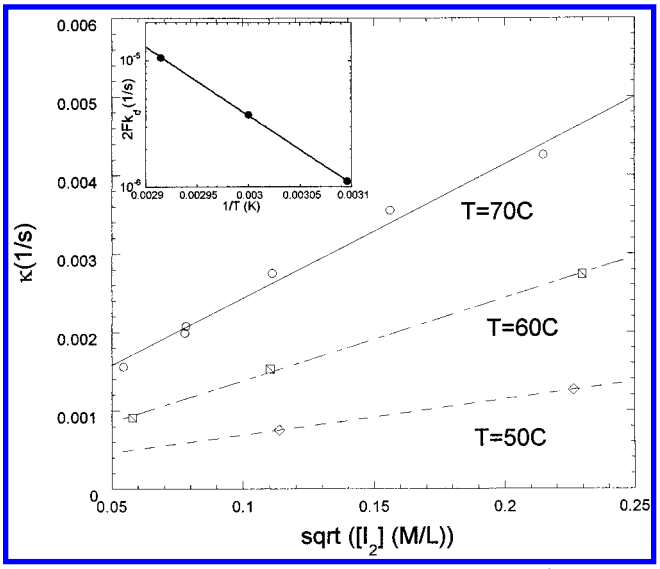

Figure 11. First-order monomer decay rates vs $\sqrt{[I_2]_0}$ for $T = 50$, 60, and 70 °C. The inset shows $2Fk_d$ vs $1/T$ for determining initiator activation energy.

obtained by SEC at equilibrium, such as where the peak mass occurs, and the fact that the distribution is skewed toward lower masses.

It is remarkable that the derivative technique of the online method, which does not involve molecular separation and is a nonequilibrium method, can supply information that approximates that obtained by an equilibrium separation technique such as SEC.

In summary, it is seen that each of the techniques for approximating evolving polymer distributions and polydispersity indices has its own virtues, weaknesses and utility. Refinement of these online polydispersity determination techniques will warrant further effort in future work. In this work no online digital filtering of data has been employed. Implementation of appropriate online filtering algorithms should lead to cleaner primary data, and hence an improvement in the quality of the various polydispersity determination techniques presented here. The ability to monitor online polydispersity, in addition to M_w, should be useful for both better understanding kinetics and mechanisms, and for industrial reactor control.

Kinetic modeling. Figure 11 shows κ vs $\sqrt{[I_2]_0}$. Figure 12a shows M_w vs $1/\sqrt{[I_2]_0}$ for the persulfate-initiated experiments at 70 °C for several conversion points, spanning $f = 0.05$ to $f = 1.0$. The linearity is quite good at all values of f down to about 0.05. Figure 12b shows the values of M_w vs $1/\sqrt{[I_2]_0}$ for $T = 50$, 60, and 70 °C data, where the values of M_w are for $f = 0$ when the linear portion of each of the M_w vs f curves (Figure 4, and the corresponding data for $T = 50$ and 70 °C experiments) is extrapolated to $f = 0$. The rationale for this is explained below.

Several features of the reaction suggest the approximate applicability of ideal kinetics; M_w and initiator decay rates vary as $1/\sqrt{[I_2]_0}$ and $\sqrt{[I_2]_0}$, respectively, and the decay of monomer during the majority of the conversion is approximately exponential. We can hence use the ideal kinetics and QSSA as a model for determining the rate constant k_d and the relationship between k_p and k_t.

Within the QSSA the monomer decay rate is given by eq 10 and [R] by eq 9. The slope of the plot of monomer decay rate vs $\sqrt{[I_2]_0}$ in Figure 11 is hence

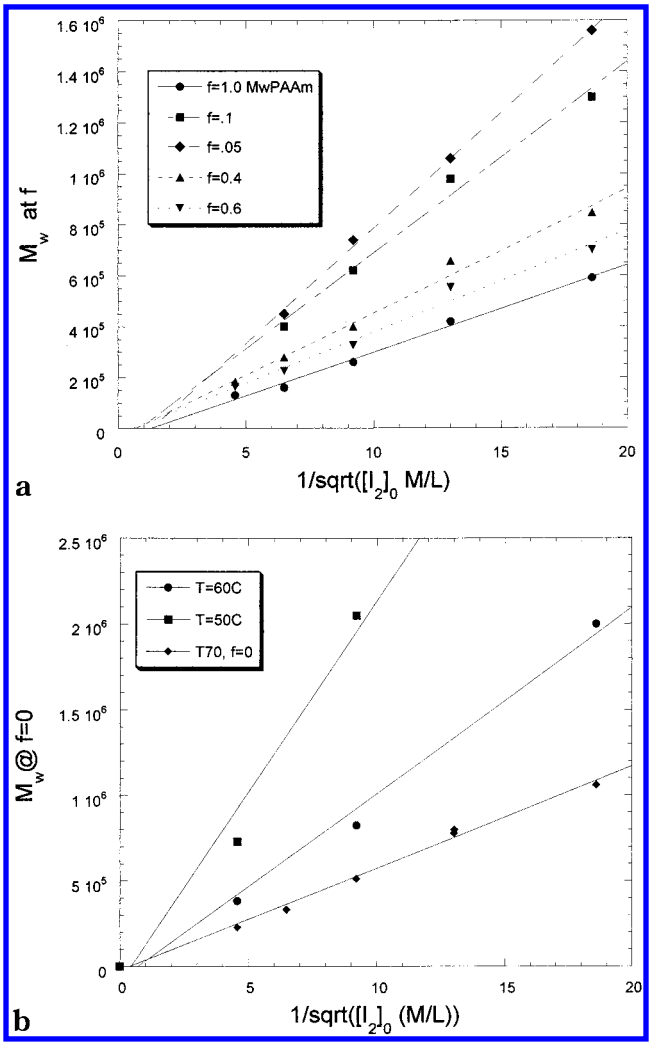

Figure 12. (a) M_w vs $1/\sqrt{[I_2]_0}$ for $T = 70$ data, spanning $f = 0.05-1$. (b) Extrapolated value for $M_w(f = 0)$ vs $1/\sqrt{[I_2]_0}$.

related to the rate constants via

$$\frac{d\kappa}{d\sqrt{[I_2]_0}} = k_p\sqrt{\frac{2Fk_d}{k_t}} \tag{25}$$

where the approximation is made that the initiator decay rate is slow compared to the time for the complete reaction, so that $[I_2]_0 \approx [I_2]$.

The kinetic chain length is the ratio of the rates of chain propagation to chain termination. When the main termination mechanism is disproportionation it is given within the QSSA as

$$\nu = \frac{k_p[m]}{k_t[R]} \tag{26}$$

When chain transfer is absent ν equals the instantaneous number-average degree of polymerization. Using eq 9 for [R], the slope is related to the rate constants by

$$\frac{d\nu}{d(1/\sqrt{[I_2]_0})} = \frac{[m]k_p}{\sqrt{2Fk_dk_t}} \tag{27}$$

Since $M_w(f)$, the cumulative weight-average mass is measured directly, instead of the kinetic chain length, a relation should be found between the last expression and M_w. When the dominant termination mechanism is disproportionation, the $M_w(f)$ is given by

$$M_w(f) = \frac{2M_{AAm}\int_0^f \nu\, df'}{f} \tag{28}$$

where M_{AAm} is the monomer mass of AAm, which is 71 g/M. The expression for kinetic chain length can be substituted

$$M_w(f) = \frac{2M_{AAm}k_p}{f\sqrt{2Fk_dk_t[I_2]_0}}\int_0^f [m](f')df' \tag{29}$$

Figure 12a shows that the proportionality of $M_w(f)$ vs $1/\sqrt{[I_2]_0}$ holds over a wide range of f. Since [m] is related to f via

$$[m] = [m]_0(1-f) \tag{30a}$$

yielding for $M_{w,inst}(f)$, when disproportionation dominates

$$M_{w,inst}(f) = 2M_{n,inst}(f=0)(1-f) \tag{30b}$$

$M_w(f)$ is approximately

$$M_w(f) \cong M_{w0}\left(1-\frac{f}{2}\right) \tag{31a}$$

where

$$M_{w0} = \frac{2M_{AAm}k_p[m]_0}{f\sqrt{2Fk_dk_t[I_2]_0}} \tag{31b}$$

Extrapolation of this expression to $f = 0$ will yield the cluster of constants

$$\frac{dM_{w0}}{d\sqrt{\frac{1}{[I_2]_0}}} = M_{AAm}\frac{k_p[m]_0}{\sqrt{Fk_dk_t/2}} \tag{32}$$

This representation is shown in Figure 12b. Hence Fk_d, and the relation between k_p and k_t, can be found by combining the derivatives in eqs 25 and 32:

$$2Fk_d = 2M_{AAm}[m]_0\frac{(d\kappa/d\sqrt{[I_2]_0})}{(dM_{w0}/d\sqrt{1/[I_2]_0})} \tag{33}$$

$$\frac{k_p^2}{k_t}\left(\frac{L}{M\times s}\right) = \frac{1}{2M_{AAm}m_0}\frac{d\kappa}{d\sqrt{[I_2]_0}}\frac{dM_{w0}}{d\sqrt{1/[I_2]_0}} \tag{34}$$

The values for $2Fk_d$ (in 1/s) following this procedure are 1.75×10^{-5}, 7.56×10^{-6}, and 1.96×10^{-6}, for $T = 70$, 60, and 50 °C, respectively. The inset to Figure 11 shows κ vs $1/T$ (T in Kelvin). According to the Arrhenius relation

$$\kappa = \kappa_0 e^{-\Delta E/k_B T} \tag{35}$$

where ΔE is the activation energy for initiator decomposition and k_B is Boltzmann's constant. The data from the inset in Figure 11 yield an activation energy $\Delta E = 101$ kJ/mol, or 24.1 kcal/mol.

Likewise, following this procedure the following values for k_p^2/k_t (in L/[M × s]) are found: 16.7 ± 0.95, 14.7 ± 1.05, and 10.6 ± 0.75, for T = 70, 60, and 50 °C, respectively. Note that if the k_t definition according to Odian[5] is used, these values must be doubled. Kinetic parameters are summarized in Table 2.

Deviations from QSSA at Early and Late Conversion. Figure 4 (and the corresponding data for T = 50 and 60 °C, not shown) show that $M_w(f)$, the cumulative weight-average polymer mass, is composed of two regimes in most cases. The first regime consists of a rapid decay of $M_w(f)$ at early conversion points, followed by an elbow region, after which there is a linear regime, usually for the rest of the conversion. The exceptions to this occur at all temperatures at the highest radical concentrations. In some of these cases, $M_w(f)$ starts low in the initial regime and then grows slightly before again decreasing to the linear plateau.

It is pointed out that the exponential sensitivity of k_d to temperature could have potentially large effects on the profile of $M_w(f)$ during early conversion for highly exo- or endothermic reactions or in systems where temperature is otherwise not well controlled. In these reactions, T did not vary significantly upon initiator addition.

Another plausible explanation for this behavior is the effect of an inhibiting agent, probably the residual diffused oxygen and perhaps residual inhibitors in the AAm. Such an agent suppresses the initial polymerization rate until it is consumed. Its effect on the molecular weight depends on the ratio of the rate constants for the inhibiting agent killing the primary radicals and killing the growing macro radicals. As long as the killing of the primary radicals is the dominant form of inhibition, this causes the few radicals that do get initiated to grow into very long molecules. If, on the other hand, the inhibiting agent is also reactive toward the initiated radicals, then it terminates the early molecules before they have a chance to grow, producing short chains at the outset of conversion.

There is higher relative error in c during the early phase of the reaction, which might have an effect on the early molecular weight results. Nevertheless, the existence of an induction period, its dependence on the initiator concentration and reaction temperature, and the much longer induction time seen when the solvent is not purged with N_2 all indicate that there is inhibition in the early part of the reaction. There is unambiguous evidence that the QSSA is not reached immediately in most cases and that a more complex initial phase is involved.

The early time behavior in Figure 11 shows that, assuming that the amount of impurity is approximately the same in each reaction, the trend seen is consistent; the higher the initiator concentration, the more quickly the impurity is consumed and the more quickly the first-order conversion of the QSSA phase is reached.

In two experiments, performed under otherwise identical conditions, one was purged with N_2 as usual, whereas the other was not purged at all. There was a longer first phase before first-order kinetics begins in the undegassed case, suggesting that the existence of impurity indeed contributes to the initial phase and that oxygen potentially comprises at least part of the impurity.

Figure 13 is a plot of the "induction period" t_i (i.e., the period over which first-order kinetics do not apply),

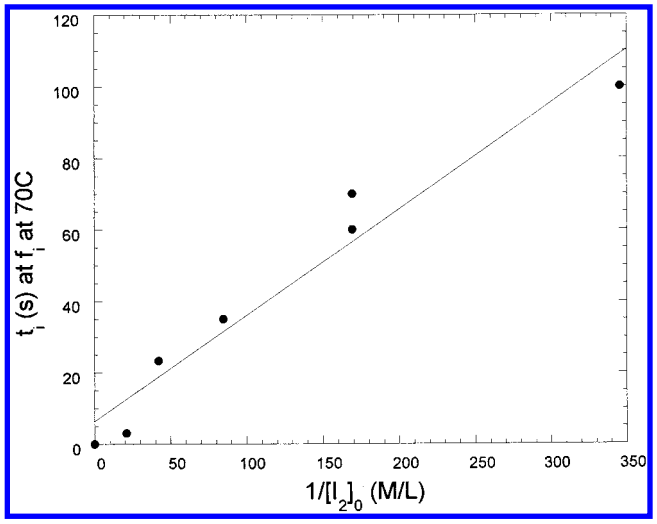

Figure 13. Induction period t_i, before onset of the QSSA regime.

found from the first-order fits to eq 17, vs $1/[I_2]$. Assuming that t_i is the time needed for sufficient amount of initiators to dissociate to neutralize the inhibiting agent, it is related to $[I_2]$, the inhibitor concentration [X] and k_d by

$$[I_2]k_d t_i = [X] \tag{36}$$

the induction time is expected to be proportional to $1/[I_2]_0$. Figure 13 shows the approximate proportionality between t_i and $1/[I_2]$. Data experiments at 60 and 50 °C follow the same trend, with longer induction times at lower temperatures consistent with lower values of k_d at these temperatures.

The dead polymer chains from the complex initial phase continue to add to the measured, cumulative $M_w(f)$, even after the main QSSA portion of the reaction has begun. Let f_i represent the value of conversion at the end of the early phase of conversion, corresponding to t_i in eq 17. Because the dependence of M_w on the inverse square root of initiator concentration holds even during much of the first phase of conversion (Figure 12a), the duration of the first phase is short compared to the long lasting QSSA phase.

In the QSSA, M_w is given by eq 28. No matter what mechanisms are operative in the first, non-QSSA phase, M_w during the QSSA phase will be given by

$$M_w(f) = \left\{\frac{f_i M_w(f_i) + M_{w0}(f - f_i)\left[1 - \frac{1}{2}(f + f_i)\right]}{f}\right\}, \quad f \geq f_i \tag{37}$$

where $M_w(f_i)$ is the cumulative weight-average mass that was produced during the first phase period $f < f_i$. We note that this form gives an elbow region with concave upward curvature even after f_i, before settling into the straight line characteristic of the QSSA. If $f_i M_w(F_i)$ is small compared to the second term in the numerator, then $M_w(f)$ will scale as $1/\sqrt{(I_0)}$. Furthermore

$$\frac{dM_w(f)}{df} = -\frac{1}{f^2}\left\{f_i(M_w(f_i) - M_{w0}) + \frac{M_{w0}}{2}(f_i^2 + f^2)\right\}, \quad f \geq f_i \tag{38}$$

If $f_i M_i$ is sufficiently small then the slope for the second regime should approach

$$\frac{dMw(f)}{df} = -\frac{M_{wo}}{2} \qquad f \gg f_i \tag{39}$$

Figure 4 shows that this linear regime is reached for all the reactions shown, and in fact, it is reached for all reactions in Table 1. The inverse square root scaling of the slope is found to hold for the $T = 60$ and 70 °C reactions, and is one-half the value found for the slope of $M_w(f = 0)$ vs $1/\sqrt{[I_2]_0}$.

Table 1 lists the values of the slopes and intercepts for the linear fits to the QSSA regime of all the reactions. If the first phase is negligible, and the reaction is wholly dominated by the QSSA, the value of the intercept should be twice the absolute value of the slope. Table 1 also lists the absolute value of the ratio of intercept to slope of M_w vs f, which allows a convenient assessment of deviations from the QSSA to be made for each reaction. All the reactions give values close to the predicted absolute value of 2.

Initiation and termination may involve more complicated reactions. A flattening of the ln[m] vs time curve is an indication of processes of higher than first-order playing a role. Two such processes have been suggested in the literature. Complex formation and the cage effect. Ishige and Hamielec[50] and Riggs and Rodriguez[51,52] consider the cage effect to be the more significant of the two.

In the cage effect, the first step of the reaction, initiator dissociation, results in two primary radicals very close to each other with a wall of solvent around them. Here they can either recombine, diffuse out of the cage, or interact with a monomer that has diffused into the cage and is initiated there. When the first and the last of these reactions compete, the initiator efficiency is proportional to the amount of monomer diffusing in. Under these conditions, the monomer concentration determines not only the propagation rate but also the initiation rate, so that eq 6b applies, rather than eq 6a. Thus, the reaction is higher order in [m].

With the cage effect the primary radicals form by

$$I_2 \xrightarrow{k_d} (2I^*) \tag{a}$$

$$(2I^*) \xrightarrow{k_{rc}} I_2 \tag{b}$$

$$m + (2I^*) \xrightarrow{k_{ic}} I^* + R \tag{c}$$

$$(2I^*) \xrightarrow{k_i} 2I^* \tag{d}$$

where (2I*) indicates a pair of radicals in close proximity after the dissociation of the initiator. The reactions using the primary radicals

$$I^* + m \xrightarrow{k_i} R_1 \tag{e}$$

$$I^* + I^* \xrightarrow{k_{Ic}} I_2 \tag{f}$$

are not part of the cage effect. Note that the combination of separated radicals (f) is second order in [I*] and the recombination of the radical within its cage (b) is first order.

It is usually assumed that[49−51] the radical diffusion out of the cage (d) is insignificant compared to both (b) and (c). When the monomer concentration is large, (c) dominates over (b). Then almost all the radicals become initiated. The initiation efficiency is close to 1 and is independent of the monomer concentration. In this regime, the cage effect is not felt. At lower monomer concentrations or alternately at later stages of the reactions when the monomer is depleted, the recombination reaction takes over so that the fraction of the monomers that are initiated is now equal to

$$F = k_{ic}[m]/k_{rc} \tag{40}$$

This is the regime where the cage effect is felt.

Toward the very end of the reaction as [m] goes toward zero, (b) cannot dominate reaction d, and so the initiator efficiency is determined solely by the rate constants for diffusion and recombination. In this regime, the reaction is again first order in [m]. However going back over to the first order is not observed or discussed in the literature, indicating that the diffusion coefficient for the radicals is small enough that the effect cannot become pronounced. Also when [m] is very low, the combination of uninitiated primary radicals can become a competitor.

Since the reaction is of $^3/_2$ order in [m] in the cage regime, the ln[m] vs t curves will flatten and ln[m] vs ln(t) will tend toward a straight line with slope −2. An alternate explanation for the cage effect by Noyes,[53,54,55] also used by Riggs and Rodriguez, has reactions b and d competing with c providing an extra efficiency. In this model, the reaction is $^5/_4$ order in the monomer concentration. These effects have also been investigated experimentally for PAAm.[56]

Parts a and b of Figure 14 show log[m] vs log(t), for reactions at $T = 70$ °C and $T = 60$ °C, respectively. In slow reactions and at high conversions (above 80−90%), these curves began to flatten. Since initiator decay times at these temperatures are longer than 10^4 s, the flattening is due more to higher order terms in the reaction than it is to a reduction in the initiator concentration. This flattening is not seen in the fastest reactions with high initiator concentrations at 70 °C and are more pronounced in the slower 60 °C reactions with low initiator concentrations. This behavior rules out the combination of diffused radicals (eq f) as an effect since that reaction, being second order in reactor concentration, would be more pronounced in the faster runs.

A reaction of order s would have

$$d[m]/dt = -[m]^s \tag{41}$$

so that

$$d(\ln[m])/d(\ln(t)) = -1/(s - 1) \tag{42}$$

during the late phase of the reaction when $[m] \ll [m]_0$. Thus, the 1.5-order mechanism discussed by Riggs and Rodriguez and by Ishige and Hamielec leads to a slope $s = -2$ whereas the 1.25-order mechanism discussed by Noyes and also used by Rigggs and Rodriguez leads to a slope of $s = -4$. Since the ln[m] vs ln(t) plots for 50 °C reactions show a slope of around 1.5 the 1.5-order mechanism provides a better explanation of the data than the alternate 1.25-order model by Noyes.

Coupled Sodium Thiosulfate/Potassium Persulfate Initiators. Table 1 lists two pairs of reactions run

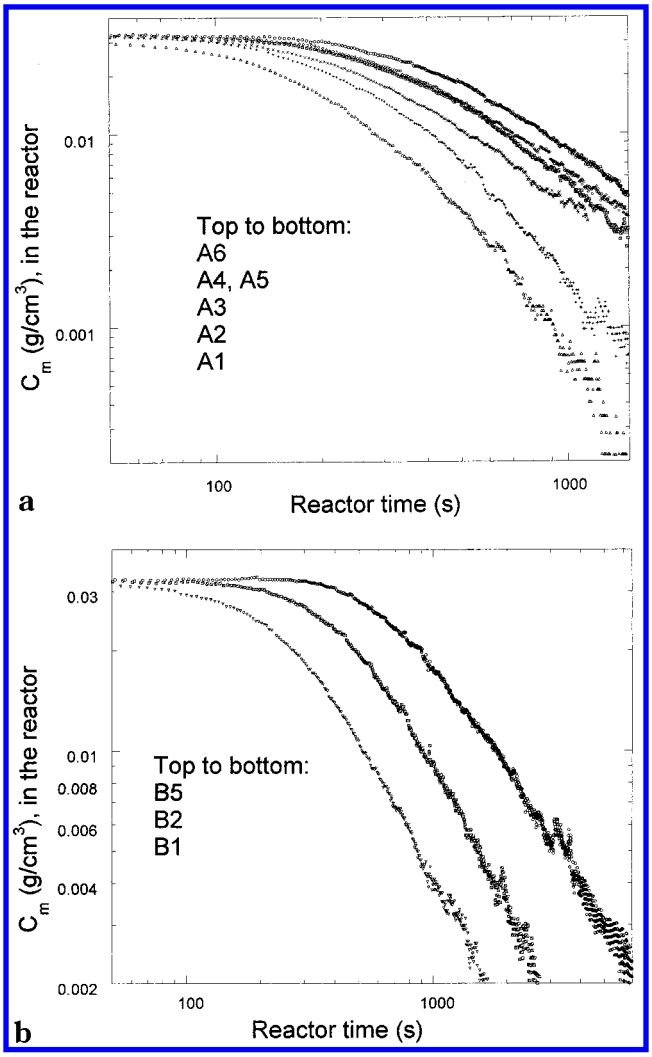

Figure 14. (a) ln[m] vs ln(t) for reactions at T = 70 °C, illustrating the higher reaction order in the latter stage of conversion. (b) ln[m] vs ln(t) for reactions at T = 60 °C, illustrating the higher reaction order in the latter stage of conversion.

under identical conditions, except that the companion reaction in each case also used the coupled thiosulfate initiator. The effect of the thiosulfate is to accelerate the reactions, but the shapes of the curves suggest that the QSSA is still applicable (see Figure 4 and linear fit parameters in Table 1). Referring to Table 1, the ratio of $M_{w,final}$ for the T = 60 °C reaction pair (B2 and B3) is 3.96. Since M_w is proportional to $1/\sqrt{[I_2]_0}$, the use of the thiosulfate/persulfate couple is equivalent to 15.7 times the concentration or persulfate that would be used, if this latter were used alone. The acceleration effect is even greater at T = 50 °C, where the ratio of final M_w is 7.5 (C2 and C3), leading to an equivalent persulfate concentration 56.3 times higher. Consistent with this trend, the lagtimes for the cases with the thiosulfate/persulfate couple are much less than those with persulfate alone.

Summary

The continuous, absolute online monitoring of acrylamide polymerization has yielded measures of polydispersity and a good description of the associated kinetics. The time-dependent signatures for conversion and M_w indicate show a square root dependence on initiator of both polymer mass at all conversion points, and of the monomer decay rate constant, indicating that the QSSA is an appropriate approximation for analyzing the reactions and obtaining the associated rate constants. Trends of the temperature dependence were also found. Deviations from the simplest form of the QSSA predictions at early conversion have been discussed in terms of impurities competing for free radical. Late conversion deviations from the QSSA are contemplated in terms of the reaction order with respect to monomer concentration changing due to cage effects. There was no evidence of either chain transfer or auto acceleration processes in any of the reactions.

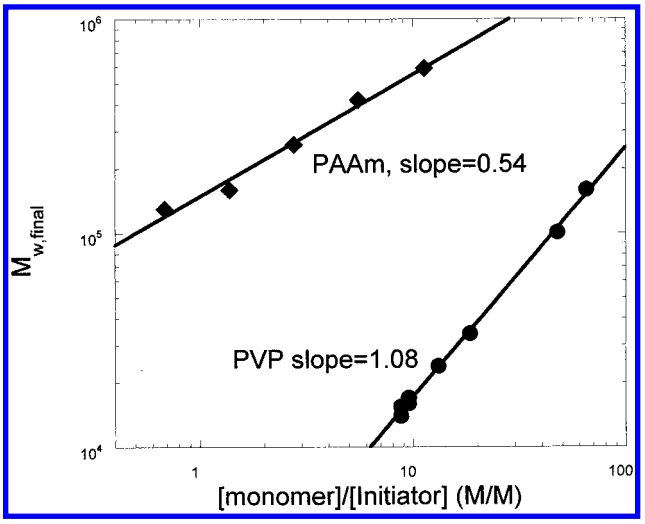

Figure 15. log($M_{w,final}$) vs log($[m]_0/[I_2]_0$) for the PAAm reactions in this work and for hydrogen peroxide initiated free radical polymerization of poly(vinylpyrrolidone) (PVP) from ref 1. The PAAm obeys ideal polymerization kinetics, whereas the PVP reaction do not.

That the QSSA is not universally applicable for chain growth polymerizations, we recall the results of ref 1, where M_w for PVP using a hydrogen peroxide initiator varied as $1/[I_2]_0$, and not as the inverse square root. Figure 15 shows a comparison of log(M_w) vs log$[I_2]_0$ for final M_w values in the T = 70 °C polyacrylamide experiments and the PVP polymerization data from ref 1, where these striking trends are seen.

It is hoped that the online technique can be used both for studying the kinetics and for studying the mechanisms of new polymerization reactions and that other well-known reactions can also be revisited.

Acknowledgment. Support from NSF CTS 9877206 and from Louisiana BoR RD-B-11 is gratefully acknowledged. J.L.B. acknowledges support from Elf Atochem Corporation.

Supporting Information Available: Text containing further details on the online method, lagtime, response time, and error considerations and figures showing $R(t)$ for UV, a typical concentration profile, a typical plot of M_w vs concentration, and a plot of the residuals. This material is available free of charge via the Internet at http://pubs.acs.org.

References and Notes

(1) Florenzano, F. H.; Streliktzki, R.; Reed, W. F. *Macromolecules* **1998**, *31*, 7226−7238.
(2) Reed, W. F. *Macromolecules* **2000**, *33*, 7165−7172.
(3) Dotson, N. A.; Galvan, R.; Laurence, R. L.; Tirrel, M. *Polymerization Process Modelling*; VCH Pub.: New York, 1996.

(4) Rodriguez, F. *Principles of Polymer Systems*, 3rd ed.; Hemisphere Pub. Corp.: Bristol, PA, 1989.
(5) Odian, G. *Principles of Polymerization*, 3rd ed.; John Wiley & Sons: New York, 1991.
(6) Bamford, C. H. *Encyclopedia of Polymer Science and Engineering, Interscience*; J. Wiley & Sons: New York, 1991; Vol. 13, pp 708−867.
(7) Howe, J. P. *J. Chem. Phys.* **1955**, *23*, 5, 899−902.
(8) Scanlan, J. *Trans. Faraday Soc.* **1956**, *52*, 1286−1291.
(9) Bamford, C. H.; Tompa, H. *Trans. Faraday Soc.* **1954**, *50*, 1097−1115.
(10) Trommsdorff, E.; Köhle, H.; Lagally, P. *Makromol. Chem.* **1948**, *1*, 169−198.
(11) Flory, *J. Am. Chem. Soc.* **1939**, *61*, 3334−3340.
(12) Bresler, S. E.; Kazbekov, E. N.; Shadrin, V. N. *Makromol. Chem.* **1974**, *175*, 2875−2880.
(13) Shen, J.; Tian, Y. *Makromol. Chem, Rapid Commun.* **1987**, *8*, 615−620.
(14) Ballard, D. G. H.; van Lienden, P. W. *Makromol. Chem.* **1972**, *154*, 177−190.
(15) Jones, C.; Brown, J. A. *Adv. Instrum.* **1983**, *38* (*Part 1, Proc. ISA Int. Conf.*), 705.
(16) Grob, R. L.; Skahan, D. J.; Dix, K.; Nielsen, K. *Process Control Qual.* **1992**, *2*, 225−235.
(17) Ehntholt, D. J.; Tayor, R. F.; Miseo, E. V. *ISA Trans.* **1993**, *32*, 2, 183−8.
(18) Storey, R. F.; Donnalley, A. B.; Maggio, T. L. *Macromolecules* **1998**, *31*, 5, 1523−1526.
(19) Mijovic, J.; Andjelic, S.; Kenny, J. M. *Polym. Adv. Technol.* **1996**, *7*, 1, 1−16.
(20) Gwosdz, C.; Francis, M. S.; Bickel, A. *Process Control Qual.* **1992**, *4*, 31−35.
(21) Scott, M. *Control Instrum.* **1991**, *23*, 3, 40−43.
(22) Penlidis, A.; MacGregor, J. F.; Hamielec, A. E. *Proc. Am. Control Conf.* **1985**, *2*, 878−880.
(23) Saltzman, R. S. *I&CS* **1994**, *67*, 2, 49−51.
(24) Kim, Y. S.; Sook, C.; Sung, P. *J. Appl. Polym. Sci.* **1995**, *57*, 3, 363−70.
(25) Paik, H. J.; Sung, N. H. *Polym. Eng. Sci.* **1994**, *34*, 1025−1032.
(26) Hansen, M. G.; Vedula, S. *Polym. Process Eng.* **1997**, *97*, 89−102.
(27) Starita, J. M.; Rohn, C. L. *Plast. Compd.* **1987**, *10*, 2, 46−51.
(28) Brand, O.; English, J. M.; Bidstrup, S. A.; Allen, M. G. *Sensors Actuators* **1997**, *1*, 121−124.
(29) Ponnuswamy, S.; Shah, S. L.; Kiparissides, C. *J. Appl. Polym. Sci.* **1986**, *32*, 3239−3253.
(30) Kotchetov, I. N.; Neckers, D. C. *J. Imaging Sci. Technol.* **1993**, *37*, 2, 156−163.
(31) Reed, W. F.; Guterman, L.; Tundo, P.; Fendler, J. H. *J. Am. Chem. Soc.* **1984**, *106*, 1897−1907.
(32) Reed, W. F. *Macromolecules* **1985**, *18*, 2402−2409.
(33) Richter, S. M.; Shinde, R. R.; Balgi, F. V.; Sevick-Muraca, E. M. *Part. Part. Syst. Charact.* **1998**, *15*, 1, 9−15.
(34) Brown, R. G. W.; Burnett, J. G.; Chow, K.; Rarity, J. G. *Proc. SPIE* **1989**, *1012*, 144−149.
(35) Povey, M. J. W. *Sensor Rev.* **1993**, *13*, 2, p 18−19.
(36) Bridge, B.; Cheng, K. H. *J. Mater. Sci. Lett.* **1987**, *6*, 2, 219−22.
(37) Schimanowski, R.; Strelitzki, R.; Reed, W. F. *Macromolecules* **1999**, *32*, 7055−7063.
(38) Rutan, S. C.; Bouveresse, E.; Andrew, K. N.; Worsfold, P. J.; Massart, D. L. *Chemom. Intell. Lab. Syst.* **1996**, *35*, 2, 199−211.
(39) Naimimohasses, R.; Barnett, D. M.; Green, D. A.; Smith, P. R. *Meas. Sci. Technol.* **1995**, *6*, 9, 1291−300.
(40) Deshpande, P. B.; Yerrapragada, S. S. *Control Eng.* **1997**, *44* (10), 55−56.
(41) Kulicke, W. M.; Kniewske, R.; Klein, J. *Prog. Polym. Sci.* **1982**, *8*, 469−484.
(42) Wang, D. W.; Thomas, W. M. *Encyclopedia of Polymer Science and Engineering*; Wiley-Interscience:, New York, 1991; Vol. 73, pp 2359−2368.
(43) Strelitzki, R.; Reed W. F. *J. Appl. Polym. Sci.* **1999**, *73*, 2359−2368.
(44) Norwood, D. P.; Reed, W. F. *Int. J. Polym. Anal. Charact.* **1997**, *4*, 99−132.
(45) Brousseau J. L.; Çatalgil-Giz, H.; Reed, W. F. *J. Appl. Polym. Sci.* **2000**, *77*, 3259−3262.
(46) Zimm, B. H. *J. Chem. Phys.* **1948**, *16*, 1093−1115.
(47) Huggins, M. L. *J. Am. Chem. Soc.* **1942**, *64*, 2716.
(48) Reed, W. F. In *Strategies for Size Exclusion Chromatography*, ACS Potschka, M.; Dubin, P., Eds.; Symposium Series 635; American Chemical Society: Washington DC, 1996; pp 7−34.
(49) Flory, P. *Principles of Polymer Chemistry*; Cornell Univ. Press: Ithaca, NY, 1972.
(50) Ishige, T.; Hamielec, A. E. *J. Appl. Polym. Sci.* **1973**, *17*, 1479−1506.
(51) Riggs, J. P.; Rodriguez, F. *J. Polym. Sci.* **1967**, *A-1*, 5, 3151−3165.
(52) Riggs, J. P.; Rodriguez, F. *J. Polym. Sci.* **1967**, *A-1*, 5, 3167−3181.
(53) Noyes, R. M. *J. Am. Chem. Soc.* **1955**, *77*, 2042−2045.
(54) Noyes, R. M. *J. Am. Chem. Soc.* **1956**, *78*, 5486−5490.
(55) Noyes, R. M. *J. Chem. Phys.* **1954**, *22*, 1349−1359.
(56) Hunkeler, D. *Macromolecules* **1991**, *24*, 2160−2171.

MA000815S